Insight into the effect of physicochemical properties on CO$_2$ absorption behavior of imidazole anion-functionalized ionic liquids

JIanni Wang
Shaoxing University

Yuxin He
Shaoxing University

Tingting Chen
Shaoxing University

Yingjie Xu (✉ xuyj@usx.edu.cn)
Shaoxing University

Bin Chen
Shaoxing University

Research Article

Additional Declarations: No competing interests reported.

Abstract

Three imidazole anion-functionalized ionic liquids (IFILs) with tributylethylphosphonium ($[P_{4442}]^+$) cation and imidazolate ($[Im]^-$), 4-methylimidazolate ($[4\text{-MeIm}]^-$), or 4-bromimidazolate ($[4\text{-BrIm}]^-$) anions were prepared to study the effect of physicochemical properties on CO_2 absorption behavior. Density (ρ), viscosity (η), speed of sound (u) of the studied IFILs were measured, and molecular volume (V_m), standard entropy (S^0), lattice energy (U_{POT}), and isentropic compressibility coefficient (κ_s) were calculated accordingly. CO_2 absorption behavior of $[P_{4442}][Im]$ at T = 313.15-333.15 K and p = 0.2 and 1 bar were investigated as an example. The results show that with the increase of temperature, ρ, η, u, and U_{POT} decrease, while V_m, S^0, and κ_s increase, due to a decrease in electrostatic interaction correspondingly. The orders of ρ, u, η, V_m, and S^0 values are as follows: $[P_{4442}][Im]$ < $[P_{4442}][4\text{-MeIm}]$ < $[P_{4442}][4\text{-BrIm}]$, while U_{POT} and κ_s are in reverse order. Interestingly, CO_2 capture capacity of IFILs is approximately linear with η or κ_s. Due to low η and high κ_s, CO_2 absorption capacity of $[P_{4442}][Im]$ is almost independent of temperature and partial pressure, as high as 0.90 mol CO_2/mol IL at 333.15 K and 0.2 bar, indicating that $[P_{4442}][Im]$ has potential applications for CO_2 absorption at high temperature and low pressure.

1 Introduction

Recently, a new type of functional ionic liquids (ILs) with imidazole-based anion such as imidazole ($[Im]^-$) and substituted imidazole ($[R\text{-Im}]^-$), namely imidazole anion-functionalized ionic liquids (IFILs), have shown good application prospects in CO_2 absorption and chemical conversion [1, 2]. In 2011, Wang et al. [3] first used $[P_{66614}][Im]$ to achieve the equimolar CO_2 capture at ambient temperature and atmospheric pressure. After that, a series of IFILs were employed as catalysts by Zhao et al. [4] to promote the reaction of atmospheric CO_2 with propargylic alcohols into various heterocyclic compounds. Among them, $[P_{4444}][2\text{-MeIm}]$ and $[P_{4444}][4\text{-MeIm}]$ exhibited high efficiencies in this reaction, which provided an good idea for ILs to catalyze CO_2 conversion at atmospheric pressure. It was well known that physicochemical property of ILs played an important role in the practical application and industrial design [5]. Wherein, density (ρ), viscosity (η), and speed of sound (u) were closely related to CO_2 capture ability and catalytic performance of CO_2 conversion by ILs [6, 7]. For example, Shi et al. [8] reported that η not only affected the CO_2 absorption rate of ILs, but also affected the CO_2 absorption capacity, and ultimately related to the catalytic CO_2 conversion performance. In addition, u of ILs could be used to obtain isentropic compressibility (κ_s) and characterize the free volume, which was related to the gas absorption performance of ILs [9−11]. Therefore, it is of great significance to study the effect physicochemical property on CO_2 absorption behavior of ILs.

In our recent work [12], four IFILs with tributylethylphosphonium ($[P_{4442}]^+$) cation and different anions including imidazolate ($[Im]^-$), 4-methylimidazolate ($[4\text{-MeIm}]^-$), 4-bromimidazolate ($[4\text{-BrIm}]^-$), and 4-nitroimidazolate ($[4\text{-NO}_2\text{Im}]^-$) were prepared and employed to capture CO_2, and the order of CO_2 absorption capacity of IFILs at T = 303.15 K and p = 1 bar was as follows: $[P_{4442}][Im]$ > $[P_{4442}][4\text{-MeIm}]$ > $[P_{4442}][4\text{-BrIm}]$ > $[P_{4442}][4\text{-NO}_2\text{Im}]$, which was compared in Figure S1 of supporting information. As plotted in Figure S1, $[P_{4442}][Im]$ showed the best capture capacity, up to 1.0 mol CO_2/mol IL, while the capture capacity of $[P_{4442}][4\text{-NO}_2\text{Im}]$ was relatively low, only about 0.3 mol CO_2/mol IL, and appeared solid near 293.15 K, indicating that the substituent at 4-position of

imidazole-based anion could significantly affect the absorption capacity of IFILs through electronic or steric effects [12]. Obviously, the anion structure of IFILs can not only affect the CO_2 absorption behavior, but also affect the physicochemical properties, such as ρ, η, and u. Therefore, it is important to investigate the physicochemical properties of IFILs, which is helpful to reveal the relationship between physicochemical properties and CO_2 absorption behavior, so as to effectively regulate the CO_2 absorption performance. Moreover, although $[P_{4442}][Im]$ has excellent CO_2 absorption capacity at T = 303.15 K and p = 1 bar, the effects of temperature and CO_2 partial pressure have not been studied in detail. As far as practical application is concerned, if $[P_{4442}][Im]$ can still maintain excellent absorption performance under relatively high temperature and low partial pressure, it may become a good candidate solvent for CO_2 capture, because CO_2 in actual flue gas generally has high temperature and low pressure properties.

To this end, based on our previous results [12], $[P_{4442}][Im]$, $[P_{4442}][4\text{-MeIm}]$, and $[P_{4442}][4\text{-BrIm}]$ were selected as typical representatives in the present work, and their physicochemical properties were studied to reveal the relationship between physicochemical properties and CO_2 absorption behavior. According to literature [13], physicochemical properties such as ρ and η have a significant effect on the CO_2 uptake of ILs. On this basis, in view of the excellent carbon capture capacity of $[P_{4442}][Im]$ at T = 303.15 K and p = 1 bar, the present work focuses on the influence of temperature and CO_2 partial pressure on its absorption behavior, and correlates the absorption behavior with its physicochemical properties. First, ρ, η, and u were measured at T = 293.15-343.15 K. According to the thermodynamic theory or empirical equations, and then the derived properties such as molecular volume (V_m), standard entropy (S^0), lattice energy (U_{POT}), and κ_s were calculated. Moreover, the influences of anion size and temperature on the physicochemical properties were discussed, and the obtained results were correlated with their CO_2 capture behavior [12]. Furthermore, CO_2 absorption behavior of $[P_{4442}][Im]$ at T = 313.15-333.15 K and p = 0.2 and 1 bar was determined to understand the influence of temperature and CO_2 partial pressure on the absorption performance, to reveal the influence of physicochemical properties on CO_2 absorption behavior of $[P_{4442}][Im]$.

2 Experiments

Chemicals

The details of the chemicals used and the purities are given in Table 1. All chemicals were used as received and obtained in highest purity grade possible. Wherein $[P_{4442}][Im]$, $[P_{4442}][4\text{-MeIm}]$, and $[P_{4442}][4\text{-BrIm}]$ three IFILs were synthesized according to our previous report [2], and the reaction equations were shown in Scheme 1. Taking the preparation of $[P_{4442}][Im]$ as an example to describe the steps, first, tributylethylphosphonium bromide ($[P_{4442}]Br$) was prepared by P_{444} and C_2H_5Br using cyclohexane as solvent under N_2 protection at reflux for 24 h. Second, tributylethylphosphonium hydroxide ($[P_{4442}][OH]$) was obtained by $[P_{4442}]Br$ through the basic anion-exchange resin activated by sodium hydroxide solution. Then, $[P_{4442}][Im]$ was synthesized through the equimolar neutralization reaction of $[P_{4442}][OH]$ and Im at room temperature for 24 h. Water in the prepared IFILs was removed at 343.15 K under vacuum. A small amount of unreacted organic raw materials in $[P_{4442}][Im]$ was removed by washing with cyclohexane, and residual cyclohexane was removed by vacuum drying. Moreover, very small amount of residual water in IFILs was removed by a freeze dryer for 48 h, and the water content in the

prepared IFILs determined by Karl Fischer titration (Mettler Toledo C20S) was lower than 500 ppm. NMR spectra of three IFILs were recorded on a Bruker AVANCE III spectrometer and shown in Figure S2. According to the purity of the raw material, NMR spectra and water content, mass fraction purity of three prepared IFILs was greater than 97%.

<div align="center">

Table 1
Sample table

</div>

Chemical name	Abbreviation or Molecular formula	CAS number	Source	Mass fraction purity	Purification method	Water content
Tributyl phosphine	P_{444}	998-40-3	Shanghai Adamas Reagent Co., Ltd	98%	None	
4-Bromimidazole	4-BrIm	2302-25-2		>98%	None	
Imidazole	Im	288-32-4	Shanghai Aladdin Reagent Co., Ltd.	99%	None	
4-Methylimidazole	4-MeIm	822-36-6		98%	None	
Bromoethane	C_2H_5Br	200-825-8		99%	None	
Cyclohexane	C_6H_{12}	110-82-7		99%	None	
Sodium hydroxide	NaOH	1310-73-2		>98%	None	
717 Basic exchange resin	-	-		-	None	
Carbon dioxide	CO_2	124-38-9	Shanghai Pu Jiang Specialty Gases Co. Ltd	>99.9%	None	
Nitrogen	N_2	7727-37-9		> 99.999%	None	
Tributylethylphosphonium imidazolate	$[P_{4442}][Im]$	1332895-10-9	Preparation in laboratory	>97%	Cyclohexane washing, vacuum drying, and freeze drying for water removal	480 ppm
Tributylethylphosphonium 4-methylimidazolate	$[P_{4442}][4-MeIm]$	2241599-92-6		>97%		485 ppm
Tributylethylphosphonium 4-bromoimidazolate	$[P_{4442}][4-BrIm]$	-		>97%		490 ppm

[a] Mass fraction purity calculated from the purity of the raw material and NMR spectra and water content of PILs

Measurement of density, viscosity, and speed of sound of IFILs

ρ, η, and u of three IFILs were simultaneously measured by an Anton Paar DSA 5000M density and sound velocity meter combined with an Anton Paar AMVn falling ball automated microviscometer. Before use, the density and sound velocity meter was calibrated with standard water and dry air, and the falling ball automated microviscometer was calibrated with standard oil. The measurement temperature of ρ and u was controlled by a built-in Peltier device with an accuracy of ± 0.01 K, and that of η was monitored by a built-in precise Peltier

thermostat with a precision of ± 0.05 K. During the determination, set the required test temperature and interval, and increase the temperature through the program, and then about 5 mL of IFILs sample was injected by using the syringe, ensuring that the sample was evenly filled with U-shaped oscillating tube and viscosity tube to avoid bubbles. The accuracy of the measurement of ρ, u, η was greater than $\pm 5.0 \times 10^{-5}$ g·cm^{-3}, ± 0.5 m·s^{-1}, and ± 0.1 mPa·s, respectively.

CO$_2$ absorption behavior of [P$_{4442}$][Im]

CO$_2$ absorption experiment of [P$_{4442}$][Im] was carried out at T = 313.15-333.15 K and p = 1 and 0.2 bar, and the experimental diagram was shown in Scheme 2. During the absorption process of p = 1 bar, a glass container with an inner diameter of 10 mm containing of about 1.00 g [P$_{4442}$][Im] was partly immersed in an oil bath to control the desired temperature, and then the dried CO$_2$ at atmospheric pressure with a flow rate of 60 ml/min was bubbled through [P$_{4442}$][Im]. The amount of CO$_2$ absorbed by [P$_{4442}$][Im] was determined at regular intervals by an electronic balance with an accuracy of ± 0.1 mg. By regulating the flow of the dried CO$_2$ and the dried N$_2$, the mixed gas of 20% CO$_2$ and 80% N$_2$ at a total flow rate of 60 ml/min was bubbled through [P$_{4442}$][Im] about 1.00 g at desired temperature to achieve the absorption of CO$_2$ at p = 0.2 bar. Other operations at p = 0.2 bar were similar to that of p = 1.0 bar.

3 Results And Discussion

Density and its Derivative Properties of IFILs

ρ, u, and η of three IFILs at T = 293.15-343.15 K are listed in Table 2. As shown in Table 2, one can see that the order of ρ at the same temperature is as follows: [P$_{4442}$][4-BrIm] > [P$_{4442}$][4-MeIm] > [P$_{4442}$][Im], which increases with the increase of the size of anion, indicating that the value of ρ can be tuned through the change the size of imidazole-based anion. Especially for [P$_{4442}$][4-BrIm], its ρ value is significantly higher than that of the other two IFILs, resulting from the electron-withdrawing effect of bromine group at 4-position, which decreases the negative charge density of the anion and reduces the electrostatic interaction between the anion and cation. Due to weaken the electrostatic interaction between anion and cation and the looseness of the structure of IFILs, ρ of IFILs decreases with the increase of temperature, which is consistent with the change rule of ρ of general liquid with temperature. According to literature [14], the relationship between ρ and temperature could be described by following empirical equation:

Table 2
Physicochemical properties of three IFILs

T (K)	ρ (g·cm⁻³)	V_m (nm³)	S^0 (J·mol⁻¹·K⁻¹)	U_{POT} (kJ·mol⁻¹)	u (m·s⁻¹)	η (mPa·s)	κ_s (10⁻⁹ Pa⁻¹)
[P₄₄₄₂][Im]							
293.15	0.96587	0.5127	668.6	397.0	1619.7	825.4	394.6
303.15	0.96011	0.5158	672.4	396.4	1586.5	397.3	413.8
313.15	0.95442	0.5188	676.2	395.8	1556.2	210.4	432.6
323.15	0.94873	0.5219	680.1	395.2	1527.6	121.0	451.7
333.15	0.94306	0.5251	684.0	394.6	1500.1	70.0	471.2
343.15	0.93738	0.5283	688.0	394.1	1473.1	47.0	491.6
[P₄₄₄₂][4-MeIm]							
293.15	1.00647	0.5151	671.6	396.5	1624.5	2115.2[a]	376.5
303.15	1.00024	0.5183	675.6	395.9	1582.2	846.7	399.4
313.15	0.99403	0.5216	679.6	395.3	1547.7	394.1	420.0
323.15	0.98789	0.5248	683.7	394.7	1516.5	202.8	440.2
333.15	0.98169	0.5281	687.8	394.1	1486.9	113.5	460.8
343.15	0.97548	0.5315	692.0	393.5	1458.5	64.4	482.0
[P₄₄₄₂][4-BrIm]							
303.15	1.18230	0.5297	689.8	393.8	1522.1	1407.7[a]	365.1
308.15	1.17878	0.5313	691.7	393.5	1503.9	926.1	375.1
313.15	1.17527	0.5329	693.7	393.2	1487.4	633.4	384.6
318.15	1.17179	0.5344	695.7	392.9	1472.5	443.6	393.6
323.15	1.16838	0.5360	697.6	392.7	1458.1	318.3	402.6
328.15	1.16486	0.5376	699.6	392.4	1444.3	233.2	411.5
333.15	1.16140	0.5392	701.6	392.1	1431.0	174.5	420.5
338.15	1.15792	0.5408	703.7	391.8	1417.9	132.9	429.5
343.15	1.15445	0.5425	705.7	391.5	1405.1	102.1	438.7

[a] Estimated by VFT equation using the parameters listed in Table 3.

$$\rho = aT + b \qquad (1)$$

where a and b were the fitted parameters. The relationship between ρ and T of three IFILs are illustrated in Fig. 1, showing satisfactory correlation results. The corresponding fitted parameters and the correlation coefficient, R^2, are listed in Table 3. Furthermore, ρ could also be used to obtain V_m of ILs [15],

Table 3
Density-temperature model parameters of three IFILs

IFILs	$10^4 a$	b	R^2
[P$_{4442}$][Im]	-5.695	1.133	0.9999
[P$_{4442}$][4-MeIm]	-6.201	1.188	0.9999
[P$_{4442}$][4-BrIm]	-6.955	1.393	0.9999

$$V_m = M/(N_A \cdot \rho) \qquad (2)$$

where M was the molar mass and N_A was Avogadro constant. The obtained V_m of three IFILs are listed in Table 2, and their values are between 0.51 and 0.55 nm^3, which is greater than that of the tetramethylguanidine imidazole anion-functionalized ILs ([TMG][Im]), with a value of 0.3066 nm^3 at 298.15 K [16]. The greater V_m values of three studied IFILs may be due to the long alkyl chain of phosphonium-based cation, which reduces the electrophilicity of the cation and prevents the anion from approaching the cation, resulting in an increase in the distance between imidazole-based anion and phosphonium-based cation and a larger molecular volume. As can be seen from Table 2 and Fig. 2a, V_m value of IFILs increases with the increase of temperature, which is attributed to the decrease of the electrostatic interaction between anion and cation with the increase of temperature. The order of V_m value is [P$_{4442}$][4-BrIm] > [P$_{4442}$][4-MeIm] > [P$_{4442}$][Im], increasing with the increase of anion size. According to literature [17], the standard entropy (S^0) of ILs has the following relationship with V_m:

$$S^0(298.15)/(J \cdot mol^{-1} \cdot K^{-1}) = 1246.5(V_m/nm^3) + 29.5 \qquad (3)$$

S^0 of the studied IFILs is calculated and shown in Table 2 accordingly, and their values are between 668 and 706 J•mol^{-1}•K^{-1}, which are much greater than those of some reported functionalized ILs at 298.15 K, such as 1-(2-methoxyethyl)-3-methylimidazolium acetic acid ([C$_1$OC$_2$mim][OAc], S^0 = 394 J•mol^{-1}•K^{-1}), 1-(2-methoxyethyl)-3-methylimidazolium propionic acid ([C$_1$OC$_2$mim][pro], S^0 = 430 J•mol^{-1}•K^{-1}), and 1-(2-ethoxyethyl)-3-methylimidazolium propionic acid ([C$_2$OC$_2$mim][Pro], S^0 = 467 J•mol^{-1}•K^{-1}) [17]. According to literature [18], S^0 value of a compound is mainly determined by its molecular structure and is generally proportional to the number of atoms in the compound. Due to the large number of atoms of the studied IFILs, they have large S^0 value. As

shown in Table 2 and Fig. 2b, the variation of S^0 of the three IFILs with temperature and the anion size is the same as V_m value.

U_{POT} was another important physicochemical property of ionic compounds, which could calculate the heat of formation or melting point [19, 20]. According to Glaser's theory [17, 21], U_{POT} of ILs can be estimated by ρ:

$$U_{\mathrm{POT}}/(\mathrm{kJ} \cdot \mathrm{mol}^{-1}) = 1981.2(\rho/M)^{1/3} + 103.8$$

4

Based on the Eq. (4), U_{POT} values of three studied IFILs are calculated and listed in Table 2, which are between 391 and 397 kJ•mol^{-1}, smaller than that of [TMG][Im] at 298.15 K (444.7 kJ•mol^{-1}) [16] and 1-alkyl-3-methyl-imidazolium tetrafluoroborate ([C$_n$mim][BF$_4$]) at 298.15 K (432 to 470 kJ·mol^{-1}) [21], suggesting that the studied IFILs may have a lower melting point. As one can see Table 2 and Fig. 2c, the order of U_{POT} value is [P$_{4442}$][4-BrIm] < [P$_{4442}$][4-MeIm] < [P$_{4442}$][Im], decreasing with the increase of anion size, which is contrary to the change of ρ V_m, and S^0. Moreover, U_{POT} value of [P$_{4442}$][4-BrIm] is significantly lower than that of the other IFILs, which may be due to the electron-withdrawing effect of bromine group at 4-position, decreasing the negative charge density of the anion and reducing the electrostatic interaction between the anion and cation, resulting in the decrease of U_{POT} value of [P$_{4442}$][4-BrIm].

Speed of sound and its derived properties of IFILs

u was an important thermodynamic property of fluid, which was related to ρ, intermolecular interaction, and free volume of liquid. Generally, the stronger interaction between molecules and the smaller free volume in the liquid, then the greater the resistance of sound wave when it travels in liquid, leading to the increase of u[22]. It can be seen from Table 2 and Fig. 3a that the order of u of three IFILs is exactly opposite to that of ρ, that is [P$_{4442}$][4-BrIm] < [P$_{4442}$][4-MeIm] < [P$_{4442}$][Im], which seems to imply that the intermolecular interaction of the studied IFILs decreases with the increase of anion size. Based on Laplace equation [23], combined with u and ρ, κ_s can be obtained through the following equation,

$$\kappa_s = \rho^{-1} u^{-2}$$

5

As listed in Table 2 and plotted in Fig. 3b, the order of κ_s is as follow: [P$_{4442}$][4-BrIm] < [P$_{4442}$][4-MeIm] < [P$_{4442}$][Im], which decreases with the increasing of anion size, indicating that the compressibility or free volume of the studied IFILs gradually decreases with the increasing of anion size. The increase of temperature weakens the interaction between anion and cation, leading to the increase of κ_s value (Table 2).

Viscosity of IFILs

As shown in Table 2, the order of η of the studied IFILs is as follows: [P$_{4442}$][4-BrIm] > [P$_{4442}$][4-MeIm] > [P$_{4442}$][Im], decreasing with the increasing of the size of anion. It can also be seen from Table 2 that η decreases rapidly with the increase of temperature, due to the decrease of the electrostatic interaction of IFILs. To better quantitatively describe the effect of temperature on η, Vogel-Fulcher-Tamman (VFT) equation is employed and expressed as follows [17]:

$$\eta = \eta_0 \exp(B/(T - T_0)) \tag{6}$$

where η_0, B, and T_0 are the fitted parameters. The fitted curves of the studied IFILs by VFT equation are shown in Fig. 4, showing that VFT equation can well describe the temperature-dependent η, and the corresponding fitting parameters of η_0, B, and T_0 are listed in Table 4.

Table 4
Fitted values of η according to the VFT equations for three IFILs

IFILs	$10\,\eta_0$ (mPa·s)	B (K)	T_0 (K)	R^2
$[P_{4442}][Im]$	0.9706	1010.91	181.45	0.9998
$[P_{4442}][4\text{-MeIm}]$	0.4220	1171.94	184.86	0.9999
$[P_{4442}][4\text{-BrIm}]$	0.4946	1207.37	185.43	0.9999

As plotted in Fig. 4, η of the studied IFILs decreases exponentially with temperature in the form of concave function, but the influence of temperature rise on η of the three IFILs is somewhat different. To reveal the influence of temperature on η behavior of the studied systems, the derivative of η with T ($\Delta\eta/\Delta T$) was calculated and also plotted in Fig. 4. As shown in Fig. 4, $\Delta\eta/\Delta T$ values of three studied IFILs are all negative, and their absolute values at the same temperature are as follows: $[P_{4442}][4\text{-BrIm}]$ > $[P_{4442}][4\text{-MeIm}]$ > $[P_{4442}][Im]$, indicating that the higher the initial η value, the more significant the decrease of its value due to temperature rise. Although the trend of η value of $[P_{4442}][Im]$ decreases with the rise of temperature is not as obvious as that of $[P_{4442}][4\text{-MeIm}]$ or $[P_{4442}][4\text{-BrIm}]$, when the temperature rises to 313.15-333.15 K, η value of $[P_{4442}][Im]$ is relatively low, which will greatly help the mass transfer of CO_2 and improve the carbon capture performance.

The effect of physicochemical properties on CO $_2$ absorption of IFILs

Based on the physicochemical properties in the present work and CO_2 capture performance of IFILs in our previous work (Figure S1) [12], the relationship between physicochemical properties and CO_2 absorption behavior will be studied next. By comparing Figs. 4 and S1, the order of η of the studied IFILs is just opposite to their CO_2 capture capacity [12], indicating that η of IFILs has an important contribution to their carbon capture performance, which is consistent with the conclusions in the literature [8]. Moreover, the order of κ_s of the studied IFILs is as follows: $[P_{4442}][4\text{-BrIm}]$ < $[P_{4442}][4\text{-MeIm}]$ < $[P_{4442}][Im]$, which is good consistent with their CO_2 capture capacity [12], indicating that that there may be a certain correlation between the free volume and carbon capture performance of the studied IFILs.

Additionally, we also try to establish the relationship between η or κ_s and CO_2 absorption capacity. As shown in Fig. 5, one can see that there is an approximate quantitative relationship between CO_2 absorption capacity of three IFILs with η or κ_s at T = 303.15 K and p = 1.0 bar. Among them, the increase in η of IFILs causes an approximate linear decrease in the CO_2 absorption capacity, while the increase in κ_s leads to an approximate linear increase in the CO_2 absorption capacity. Therefore, the obtained results in the present work further confirm that κ_s reflected the free volume of IFILs is related to the gas absorption performance [6, 24], and the higher κ_s

values, the greater free volume and the better CO_2 absorption capacity. Moreover, the mass transfer rate and diffusion ability of CO_2 in ILs are significantly affected by η of ILs [25, 26], which is also related to the CO_2 absorption capacity [8]. Generally, the higher η is, the worse the mass transfer and diffusion ability of CO_2 is, resulting in the decrease of the mutual contact and interaction between gas phase and liquid phase, thus reducing the CO_2 absorption capacity of IFILs. As illustrated in Fig. 5, a consequence of lower η and higher κ_s, $[P_{4442}][Im]$ exhibits the better CO_2 absorption capacity, so it is worth studying the influence of temperature and CO_2 partial pressure on the absorption capacity of $[P_{4442}][Im]$.

The effect of temperature and partial pressure on CO $_2$ absorption of [P $_{4442}$][Im]

CO_2 absorption behavior of $[P_{4442}][Im]$ at $T = 313.15\text{-}333.15$ K and $p = 1.0$ bar were plotted in Fig. 6a, compared with those of $T = 303.15$ K [12]. As can be seen in Fig. 6a, the saturated CO_2 absorption capacity decreases slightly with the temperature, which is attributed to the exothermic absorption process [3], but the amount of decrease is not obvious. For example, the saturated CO_2 absorption capacity at $T = 313.15$ K is similar to that of at $T = 303.15$ K. Even when the temperature rises to 333.15 K, the saturated CO_2 absorption capacity is still greater than 0.9 mol CO_2/mol IL, similar to that of metal chelate-based ionic liquids (ChILs) [27], which are famous for the efficient absorption of CO_2 at high temperature [7]. Moreover, CO_2 absorption behavior of $[P_{4442}][Im]$ at $T = 313.15\text{-}333.15$ K and $p = 0.2$ bar were shown in Fig. 6b, compared with those of $T = 313.15$ K and $p = 1.0$ bar. As we can see, when the CO_2 partial pressure is 0.2 bar, $[P_{4442}][Im]$ also shows good absorption performance. As plotted in Fig. 6b, the CO_2 absorption behavior of $[P_{4442}][Im]$ at $T = 313.15$ K and $p = 0.2$ bar are almost consistent with those at $T = 313.15$ K and $p = 1.0$ bar. It is exciting that the CO_2 saturation absorption of $[P_{4442}][Im]$ at $T = 333.15$ K and $p = 0.2$ bar is close to 0.9 mol CO_2/mol IL, which means that $[P_{4442}][Im]$ can be potentially applied to efficient CO_2 capture at relatively high temperature and low partial pressure.

Table 5 presents a comparison of CO_2 absorption capacity of $[P_{4442}][Im]$ with that of other functionalized ILs or metal ChILs reported in the literature. As can be seen from Table 5, although CO_2 absorption capacity of $[P_{4442}]$ $[Im]$ at $T = 313.15$ K and $p = 1.0$ bar and $[P_{66614}][Im]$ at $T = 296.2$ K and $p = 1.0$ bar is almost the same [3], $[P_{4442}]$ $[Im]$ still maintains good absorption performance at higher temperature and lower partial pressure. Moreover, CO_2 absorption capacity of $[P_{4442}][Im]$ at high temperature and low pressure is almost the same as that of $[P_{4442}][Suc]$ [28], suggesting that $[P_{4442}][Im]$ may be more suitable for carbon capture under actual conditions. It can also be seen from Table 5 that CO_2 absorption capacity of $[P_{4442}][Im]$ is better than that of carbanion-derived superbase-derived task-specific ILs (STSILs) such as $[P_{66614}][MN]$, $[P_{4444}][MN]$, and $[P_{4442}][MN]$, which are proposed by Yang and co-workers recently for efficient CO_2 chemisorption via a carboxylic acid formation pathway [29]. Notably, the studied IFILs for efficient CO_2 chemisorption via a carbonate formation pathway [3, 12], so the final product formed by the studied IFILs absorbing CO_2 is different from that of STSILs [29], and the presence of carboxyl hydrogen in the latter product is easy to cause the formation of intermolecular hydrogen bond network structure after the absorption of CO_2 by STSILs and leads to a sharp increase in η of the system and the decrease of CO_2 absorption efficiency [33−36]. Therefore, this may be an important reason why CO_2 absorption capacity of $[P_{4442}]$ $[Im]$ is better than that of STSILs [29]. Moreover, by comparing the absorption listed in Table 5, it can be found that CO_2 absorption capacity of $[P_{4442}][Im]$ is greater than that of CHILs absorbed CO_2 through the chelate-based

cation between Li^+ and polyamines [8, 30], and is similar to that of dual functional CHILs [7, 31, 32], which can capture CO_2 through the chelate-based cation and functionalized anion simultaneously and is famous for its applicability to carbon capture at high temperature and low pressure. As a result, $[P_{4442}][Im]$ shows satisfactory absorption performance compared with some typical functionalized ILs reported in the literature.

Table 5

Comparison of CO_2 absorption by $[P_{4442}][Im]$ and some reported ILs

ILs	T (K)	p (bar)	Absorption capacity (mole CO_2 per mole IL)	Ref.
$[P_{4442}][Im]$	313.15	1.0	0.98	This work
$[P_{4442}][Im]$	323.15	1.0	0.93	This work
$[P_{4442}][Im]$	333.15	1.0	0.91	This work
$[P_{4442}][Im]$	313.15	0.2	1.00	This work
$[P_{4442}][Im]$	323.15	0.2	0.96	This work
$[P_{4442}][Im]$	333.15	0.2	0.88	This work
$[P_{4442}][Im]$	303.15	1.0	1.00	[12]
$[P_{66614}][Im]$	296.2	1.0	1.00	[3]
$[P_{4442}][Suc]$	333.15	0.1	0.88	[28]
$[P_{66614}][MN]$	298	1.0	0.84	[29]
$[P_{4444}][MN]$	298	1.0	0.86	[29]
$[P_{4442}][MN]$	298	1.0	0.86	[29]
$[P_{66614}][MMN]$	298	1.0	0.35	[29]
$[Li(DOBA)][Tf_2N]$	333.2	1.0	0.90	[30]
$[Li(DETA)][Tf_2N]$	353.2	0.1	0.66	[8]
$[Li(TETA)][Tf_2N]$	353.2	0.1	0.70	[8]
$[Li(TEPA)][Tf_2N]$	353.2	0.1	0.72	[8]
$[Li(TEG)][Tf_2N]$	353.2	0.1	0.01	[8]
$[Li(TTEG)][Tf_2N]$	353.2	0.1	0.02	[8]
$[K(18\text{-crown-}6)][Pro]$	298.2	1.0	0.99	[31]
$[K(MEA)_2][Im]$	333.2	1.0	0.76	[32]
$[K(DLAMP)_2][Im]$	333.2	1.0	1.00	[7]
$K(AMB)_2][Im]$	333.2	1.0	1.09	[7]
$[K(AMP)_2][Im]$	333.2	1.0	1.19	[7]

It is well known that CO_2 chemisorption process by ILs is an exothermic reaction [3, 33], so CO_2 capture capacity of ILs usually decreases dramatically with an increase in temperature. In addition, the decrease of CO_2 partial pressure will reduce the contact probability and interaction between CO_2 and ILs, also resulting in the decrease of absorption. In view of CO_2 absorption behavior of $[P_{4442}][Im]$ measured in the present experiment, it is worth exploring the reason why $[P_{4442}][Im]$ still has excellent carbon capture performance at relatively high temperature and relatively CO_2 low pressure. As illustrated in Fig. 5, CO_2 absorption capacity of the studied IFILs increases with the increase of κ_s and decreases with the increase of η, indicating that the increase of κ_s and the decrease of η may be good for CO_2 absorption capacity of IFILs. As shown in Figs. 3b and 4, κ_s of $[P_{4442}][Im]$ increases linearly with temperature, while η of $[P_{4442}][Im]$ decreases exponentially with temperature. Moreover, one can be seen in Table 2 and Fig. 4 that η value of $[P_{4442}][Im]$ decreases from 210.4 to 70.0 mPa•s within the temperature range of 313.15 to 333.15 K, and the corresponding $\Delta\eta/\Delta T$ value of $[P_{4442}][Im]$ increases from about − 15 to -3, resulting from the significant decrease of electrostatic interaction between anion and cation in $[P_{4442}][Im]$ and the dissociation of hydrogen bond network, which reduces the attraction of cation to anion and can promote the nucleophilic interaction between anion and CO_2 to maintain the capture of CO_2 effectively. Therefore, we believe that the influence of temperature on the carbon capture performance of functionalized ILs is the result of competition between exothermic effect of absorption process and the increase of molecular free volume and the decrease of η. If the increase of temperature leads to the increase of free volume and the rapid decrease of viscosity of ILs, and promotes the increase of CO_2 absorption, it will just make up for the decrease of CO_2 absorption caused by the exothermic effect of absorption process, then the CO_2 absorption capacity of ILs may remain basically unchanged with the increase of temperature or less affected by temperature. As for $[P_{4442}][Im]$, it can be seen from Figs. 3b and 4 that its free volume increases and its viscosity decreases rapidly with the increase of temperature, and they promote the CO_2 absorption synergistically, which compensates for the decrease of the CO_2 absorption effectively brought by the exothermic effect of the reaction between $[P_{4442}][Im]$ and CO_2, so as to maintain the CO_2 absorption capacity of $[P_{4442}][Im]$ unchanged with the increase of temperature.

Naturally, $[P_{4442}][Im]$ with a larger free volume and a lower η makes it have a more loose internal structure, so even when CO_2 partial pressure is 0.2 bar, CO_2 can still shuttle freely in the molecular interior of $[P_{4442}][Im]$, and react with $[P_{4442}][Im]$ quickly, thus maintaining a high absorption capacity. Based on the results of present study and our previous study [12], it can be considered that the strong alkalinity of $[Im]^-$ makes $[P_{4442}][Im]$ show excellent CO_2 absorption capacity, moreover, $P_{4442}][Im]$ with a larger free volume and a lower η makes it still have good CO_2 absorption performance at higher temperature and lower partial pressure.

4 Conclusions

Herein, on the basis of the density, viscosity (η), and speed of sound of $[P_{4442}][Im]$, $[P_{4442}][4\text{-MeIm}]$, and $[P_{4442}][4\text{-BrIm}]$ three IFILs, a series of derivative properties are obtained by thermodynamic model, focusing on the effect of physicochemical properties on CO_2 absorption behavior of IFILs. The results show CO_2 absorption capacity of three IFILs at T = 303.15 K and p = 1.0 bar shows an approximate linear relationship with the increase of

isentropic compressibility coefficient (κ_s) and the decrease of η. Among them, [P$_{4442}$][Im] with greater κ_s and lower η exhibits better CO_2 absorption capacity at T = 303.15 K and p = 0.2 bar. Moreover, CO_2 absorption capacity of [P$_{4442}$][Im] at T = 313.15-333.15 K and p = 0.2 bar is close to 0.9 mol CO_2/mol IL, and is less affected by temperature and CO_2 partial pressure. Based on physicochemical properties and the relationship with CO_2 absorption of IFILs, this study believes that it is due to the fact that the free volume of [P$_{4442}$][Im] increases with temperature and η decreases rapidly with temperature, so that CO_2 can still freely diffuse in the molecular interior at higher temperature and lower partial pressure, and react with basic anions to make up for the reduction of CO_2 absorption caused by exothermic effect in the absorption process, so as to ensure that [P$_{4442}$][Im] can still maintain excellent absorption performance at high temperature and low pressure. The present results will provide a way to build the relationship between IFILs and carbon capture performance.

Declarations

Competing interests

The authors declare no competing interests.

Acknowledgements

References

1. Fu, X., Tang, X., Chen, T., Xu, Y., Luo, X., Lu, Y., Wang, X., Qin, D., Zhang, L. Understanding of the interactions between azole-anion-based ionic liquids and 2-methyl-3-butyn-2-ol from the experimental perspective: the cage effect. Phys. Chem. Chem. Phys. **24**, 12550-12562 (2022).

2. Liu, J., Tang, X., Lu, H., Xu, Y. Insight into the interactions between azole-anion-based ionic liquids and propargylic alcohol: influence on the carboxylative cyclization of propargylic alcohol with carbon dioxide. ACS Sustainable Chem. Eng. **9**, 5050-5060 (2021).

3. Wang, C., Luo, X., Luo, H., Jiang, D-E., Li, H., Dai, S. Tuning the basicity of ionic liquids for equimolar CO_2 capture. Angew. Chem. Int. Ed. **50**, 4918-4922 (2011).

4. Zhao, Y., Wu, Y., Yuan, G., Hao, L., Gao, X., Yang, Z., Yu, B., Zhang, H., Liu, Z. Azole-anion-based aprotic ionic liquids: functional solvents for atmospheric CO_2 transformation into various heterocyclic compounds. Chem.-Asian J. **11**, 2735-2740 (2016).

5. Candia-Lomelí, M., Covarrubias-Garcia, I., Aizpuru, A., Arriaga, S. Preparation and physicochemical characterization of deep eutectic solvents and ionic liquids for the potential absorption and biodegradation of styrene vapors. J. Hazard. Mater. **441**, 129835 (2023).

6. Chen, T., Wu, X., Xu, Y. Effects of the structure on physicochemical properties and CO_2 absorption of hydroxypyridine anion-based protic ionic liquids. J. Mol. Liq. **362**, 119743 (2022).

7. Zema, Z.A., Chen, T., Shu, H., Xu, Y. Tuning the CO_2 absorption and physicochemical properties of K$^+$ chelated dual functional ionic liquids by changing the structure of primary alkanolamine ligands. J. Mol. Liq. **344**,

117983 (2021).

8. Shi, G., Zhao, H., Chen, K., Lin, W., Li, H., Wang, C. Efficient capture of CO_2 from flue gas at high temperature by tunable polyamine-based hybrid ionic liquids. AIChE J. **66**, e16779 (2020).

9. Wenny, M.B., Molinari, N., Slavney, A.H., Thapa, S., Lee, B., Kozinsky, B., Mason, J.A. Understanding relationships between free volume and oxygen absorption in ionic liquids. J. Phys. Chem. B **126**, 1268-1274 (2022).

10. Ramkumar, V., Gardas, R.L. Thermophysical properties and carbon dioxide absorption studies of guanidinium-based carboxylate ionic liquids. J. Chem. Eng. Data **64**, 4844-4855 (2019).

11. García-Gutiérrez, P., Jacquemin, J., Mccrellis, C., Dimitriou, I., Taylor, S.F.R., Hardacre, C., Allen, R.W.K. Techno-economic feasibility of selective CO_2 capture processes from biogas streams using ionic liquids as physical absorbents. Energy Fuels **30**, 5052-5064 (2016).

12. He, Y., Wang, J., Chen, T., Xu, Y. Effects of substituents on carbon capture properties of imidazole anion-functionalized ionic liquids. Energy Environmental Protection **36**, 60-65 (2022) (in Chinese).

13. Krishnan, A., Gopinath, K.P., Vo, D.V.N., Malolan, R., Nagarajan, V.M., Arun, J. Ionic liquids, deep eutectic solvents and liquid polymers as green solvents in carbon capture technologies: a review. Environ. Chem. Lett. **18**, 2031-2054 (2020).

14. Yang, J., Lu, X., Gui, J., Xu, W. A new theory for ionic liquids—the interstice Model Part 1. The density and surface tension of ionic liquid EMISE. Green Chem. **6**, 541-543 (2004).

15. Ma, D., Zhu, C., Fu, T., Ma, Y., Yuan, X. Performance and pressure drop of CO_2 absorption into task-specific and halide-free ionic liquids in a microchannel. AIChE J. **68**, e17613 (2022).

16. Chen, J., Chen, L., Xu, Y. Properties of pure 1, 1, 3, 3-tetramethylguanidine imidazole ionic liquid and its binary mixtures with alcohols at T = (293.15 to 313.15) K. J. Chem. Thermodyn. **88**, 110-120 (2015).

17. Wang, J., Li, Y., Guo, C., Zhao, Y., Tong, J. Viscosity and electrical conductivity of ether-functionalized ionic liquids-[C_1OC_2mim][OAc], [C_1OC_2mim][Pro] and [C_2OC_2mim][Pro]. J. Mol. Liq. **349**, 118200 (2022).

18. Mu, L., He, H. Prediction of standard absolute entropies for gaseous organic compounds. Chemom. Intell. Lab. Syst. **112**, 41-47 (2012).

19. Zhang, D., Li, B., Hong, M., Kong, Y., Tong, J. Synthesis and characterization of physicochemical properties of new ether-functionalized amino acid ionic liquids. J. Mol. Liq. **304**, 112718 (2020).

20. Wang, J., Jiang, H., Liu, Y., Hu, Y. Density and surface tension of pure 1-ethyl-3-methylimidazolium L-lactate ionic liquid and its binary mixtures with water. J. Chem. Thermodyn. **43**, 800-804 (2011).

21. Glasser, L. Lattice and phase transition thermodynamics of ionic liquids. Thermochim. Acta **421**, 87-93 (2004).

22. Wu, K., Chen, Q., He, C. Speed of sound of ionic liquids: database, estimation, and its application for thermal conductivity prediction. AIChE J. **60**, 1120-1131 (2014).

23. Keshapolla, D., Srinivasarao, K., Gardas, R.L. Influence of temperature and alkyl chain length on physicochemical properties of trihexyl- and trioctylammonium based protic ionic liquids. J. Chem. Thermodyn. **133**, 170-180 (2019).

24. Das, I., Swami, K.R., Gardas, R.L. Influence of alkyl substituent on thermophysical properties and CO_2 absorption studies of diethylenetriamine-based ionic liquids. J. Mol. Liq. **371**, 121114 (2023).

25. Zhang, X., Bao, D., Huang, Y., Dong, H., Zhang, X., Zhang, S. Gas−liquid mass-transfer properties in CO_2 absorption system with ionic liquids. AIChE J. **60**, 2929-2939 (2014).

26. Sánchez, L.G., Meindersma, G.W., De Haan, A.B. Kinetics of absorption of CO_2 in amino-functionalized ionic liquids. Chem. Eng. J. **16**, 1104-1115 (2011).

27. Zhang, S., Wang, X., Yao, J., Li, H. Electron paramagnetic resonance studies of the chelate-based ionic liquid in different solvents. Green Energy Environ. **5**, 341-346 (2020).

28. Huang, Y., Cui, G., Zhao, Y., Wang, H., Li, Z., Dai, S., Wang, J. Preorganization and cooperation for highly efficient and reversible capture of low-concentration CO_2 by ionic liquids. Angew. Chem. Int. Ed. **56**, 13293-13297 (2017).

29. Suo, X., Fu, Y., Do-Thanh, C.L., Qiu, L.-Q., Jiang, D.-E., Mahurin, S.M., Yang, Z, Dai, S. CO_2 Chemisorption behavior in conjugated carbanion-derived ionic liquids via carboxylic acid formation. J. Am. Chem. Soc. **144**, 21658-21663 (2022).

30. Wang, C., Guo, Y., Zhu, X., Cui, G., Li, H., Dai, S. Highly efficient CO_2 capture by tunable alkanolamine-based ionic liquids with multidentate cation coordination Chem. Commun. **48**, 6526-6528 (2012).

31. Yang, Z.-Z., Jiang, D.-E., Zhu, X., Tian, C., Brown, S., Do-Thanh, C.L., He, L.-N., Dai, S. Coordination effect-regulated CO_2 capture with an alkali metal onium salts/crown ether system. Green Chem. **16**, 253-258 (2014).

32. Shu, H., Xu, Y. Tuning the strength of cation coordination interactions of dual functional ionic liquids for improving CO_2 capture performance. Int. J. Greenhouse Gas Control **94**, 102934 (2020).

33. Gutowski, K.E., Maginn, E.J. Amine-functionalized task-specific ionic liquids: a mechanistic explanation for the dramatic increase in viscosity upon complexation with CO_2 from molecular simulation. J. Am. Chem. Soc. **130**, 14690-14704 (2008).

34. Luo, X., Fan, X., Shi, G., Li, H., Wang, C. Decreasing the viscosity in CO_2 capture by amino-functionalized ionic liquids through the formation of intramolecular hydrogen bond. J. Phys. Chem. B **120**, 2807-2813 (2016).

35. Goodrich, B.F., de la Fuente, J.C., Gurkan, B.E., Lopez, Z.K., Price, E.A., Huang, Y., Brennecke, J.F. Effect of water and temperature on absorption of CO_2 by amine-functionalized anion-tethered ionic liquids. J. Phys. Chem. B **115**, 9140-9150 (2011).

36. Brennecke, J.F., Gurkan, B.E. Ionic liquids for CO_2 capture and emission reduction. J. Phys. Chem. Lett. **1**, 3459-3464 (2010).

Schemes

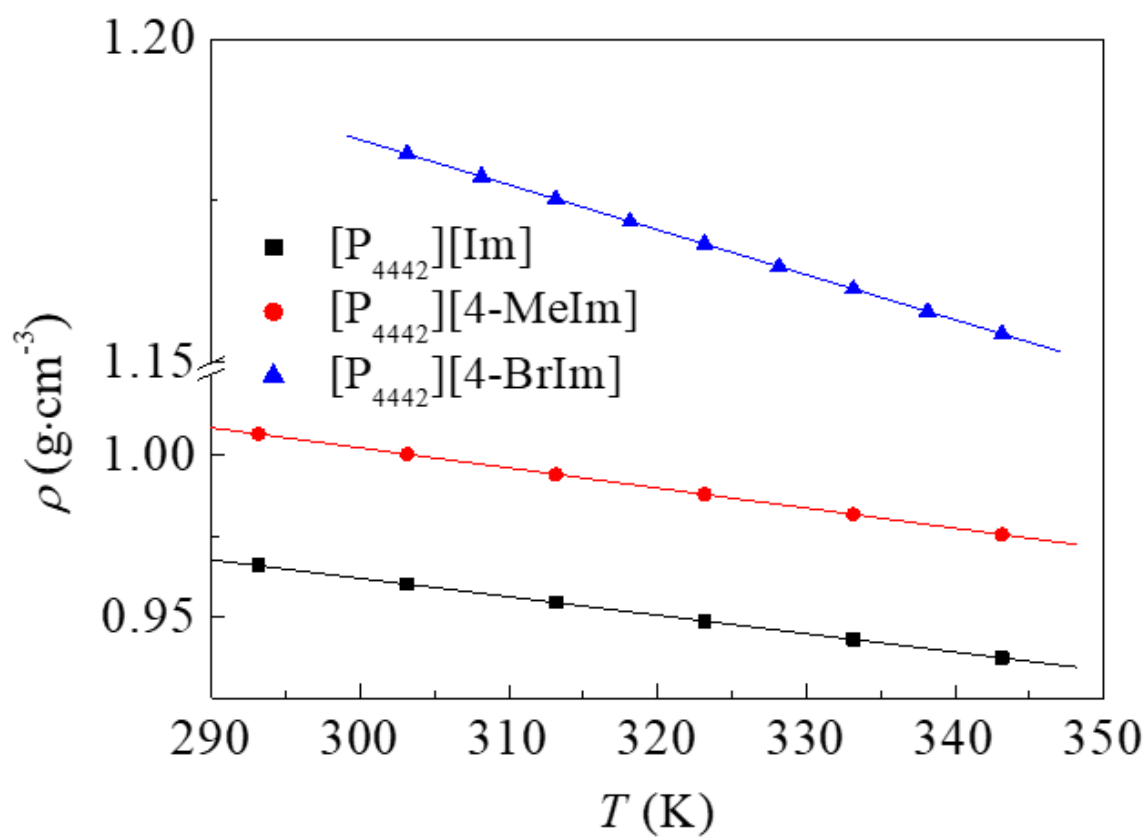Schemes 1 and 2 are available in the Supplementary Files section

Figures

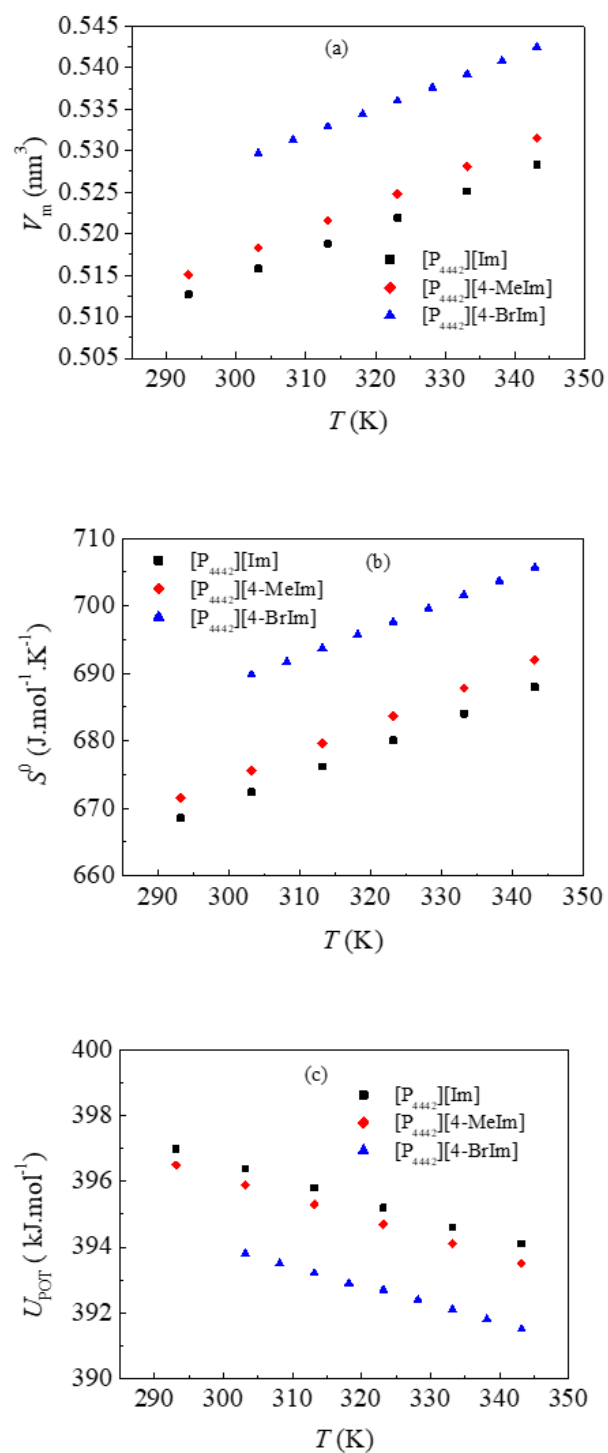**Figure 1**

The relationships of $\rho \sim T$ of three IFILs.

Figure 2

Plot of V_m against T (a), S^0 against T (b), and U_{POT} against T (c) for three IFILs.
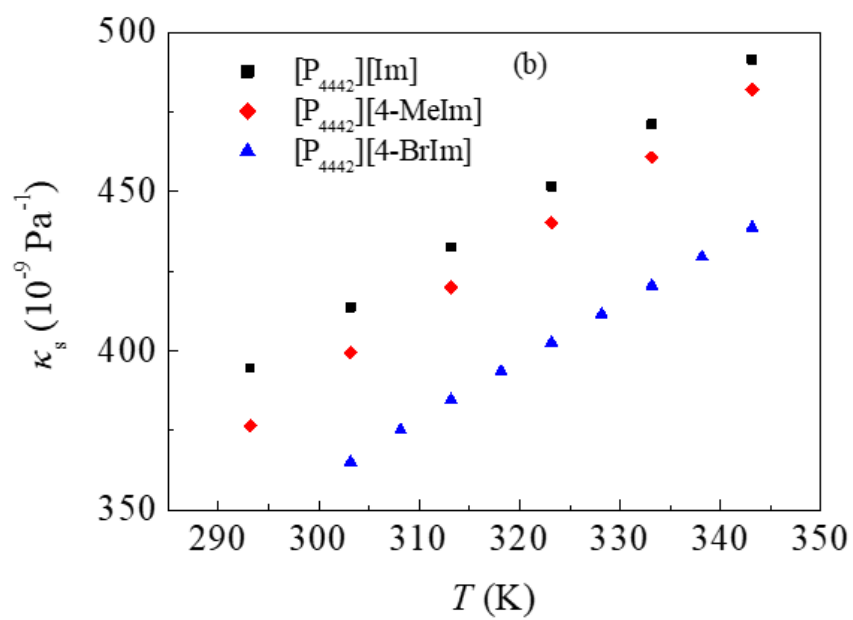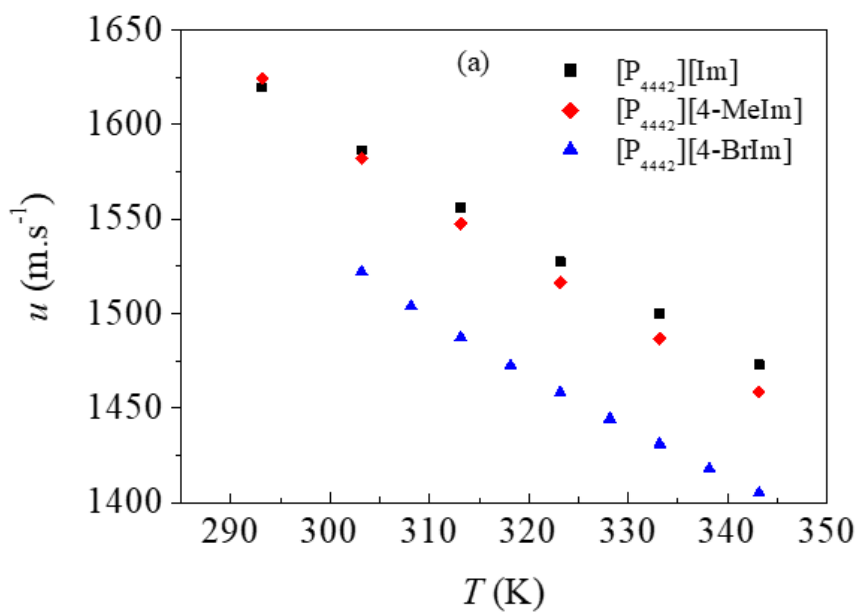
Figure 3

Plot of u against T (a) and κ_s against T (b) for three IFILs.
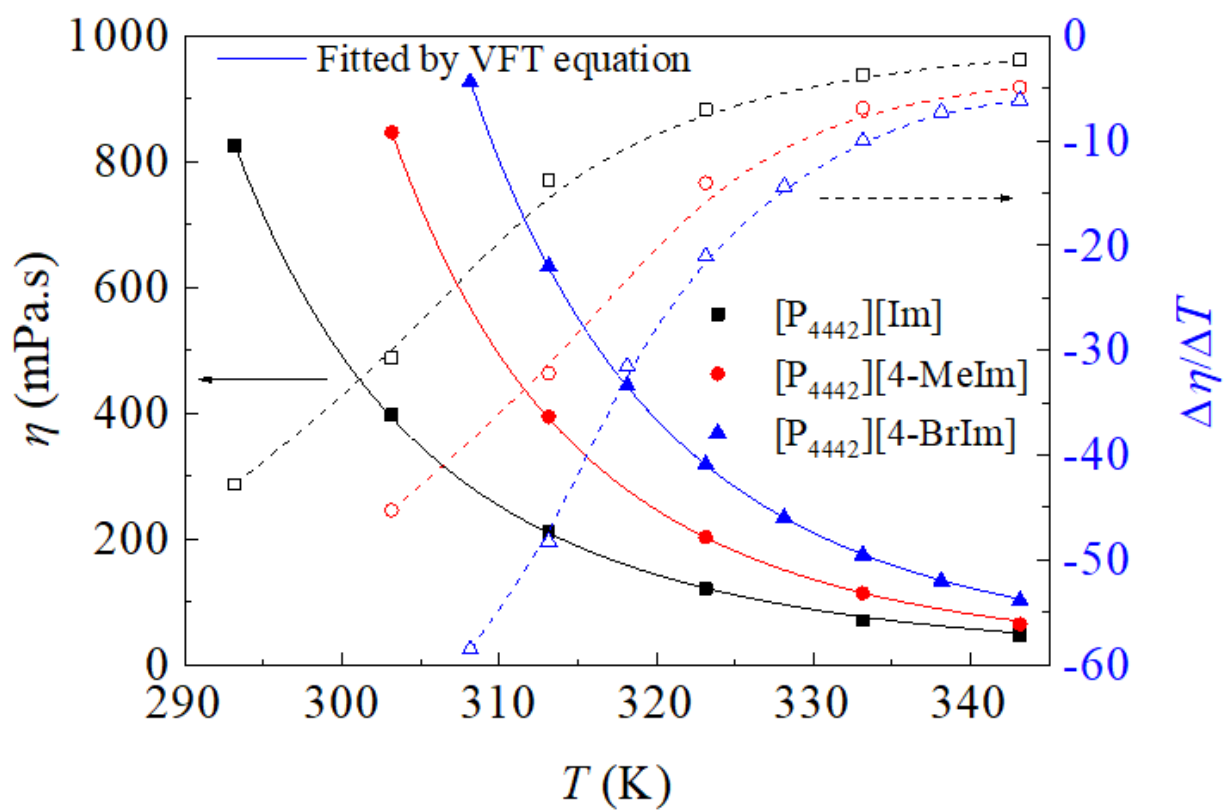
Figure 4

Plot of η against T by VFT equation and their derivative with T for three IFILs.
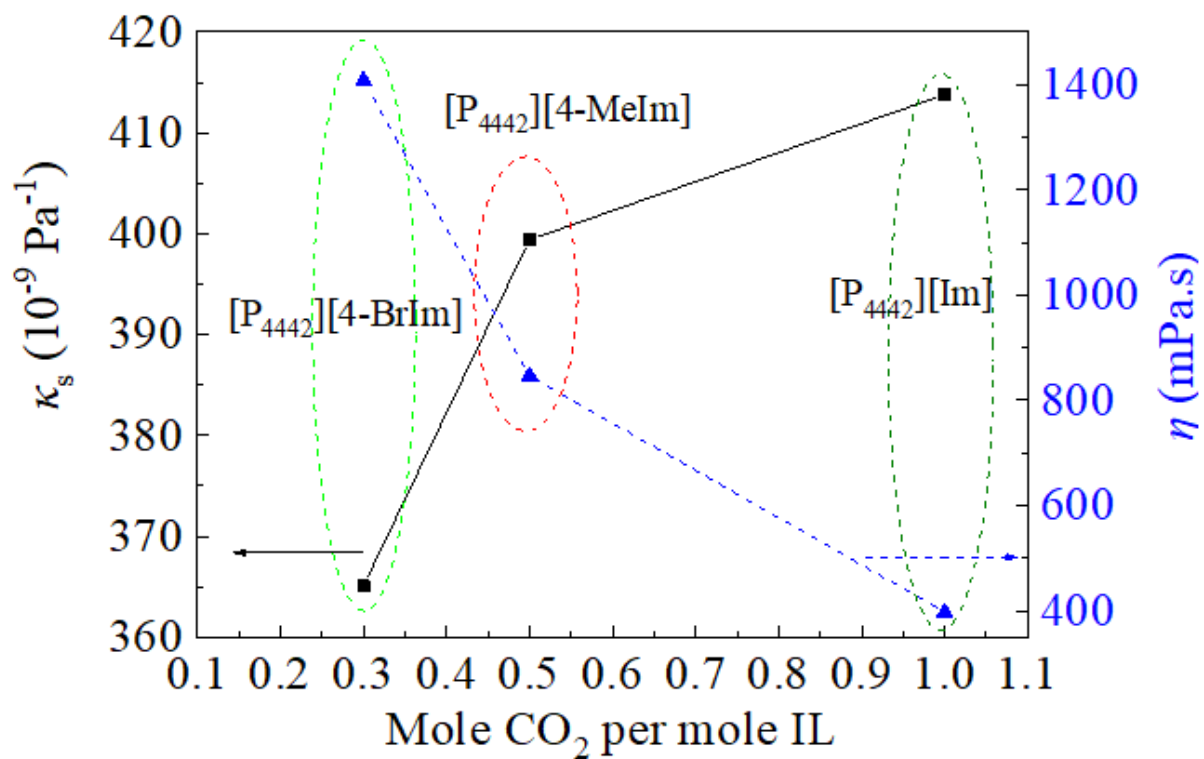
Figure 5

The relationship between CO_2 absorption capacity (T = 303.15 K and p = 1.0 bar) with κ_s and η (T = 303.15 K) of three IFILs.
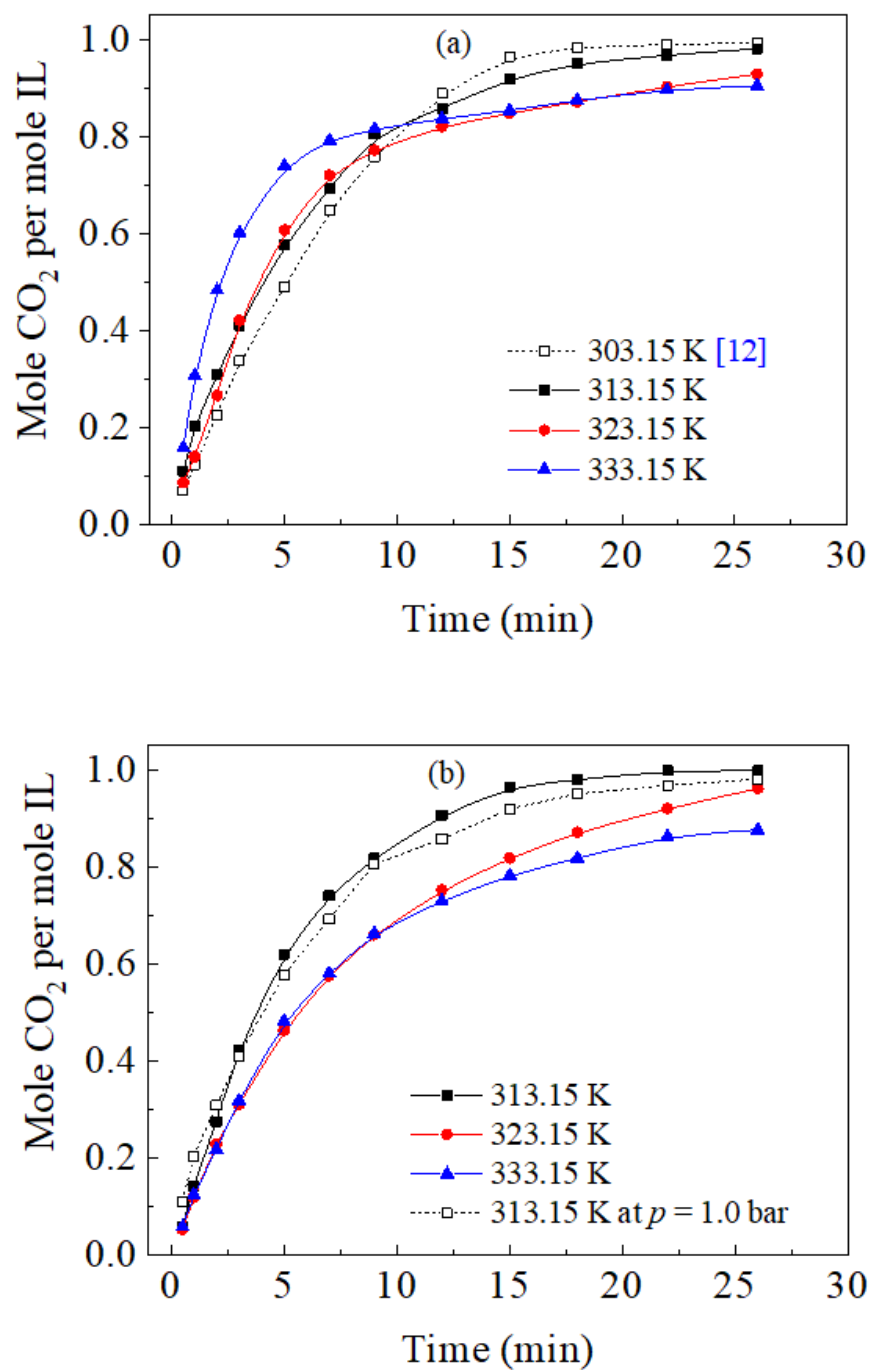
Figure 6

The effect of temperature of CO_2 absorption behavior of $[P_{4442}][Im]$ at p = 1.0 bar (a) and p = 0.2 bar (b).

Supplementary Files

This is a list of supplementary files associated with this preprint. Click to download.

- Scheme1.png
- Scheme2.png

- SupplementaryInformation.pdf